First-principles study of NO_x and SO_2 adsorption onto $SnO_2(110)$ and SnO_2 nanoparticles

Joan Daniel Prades García

Dr. Albert Cirera Hernàndez, Departament d'Electrònica, Universitat de Barcelona

***Abstract* — An ab initio study of the adsorption of NO_x and SO_2 onto $SnO_2(110)$ surfaces is presented and related to gas-sensing applications. Using first-principles calculations (DFT-GGA approximation) the most relevant NO and NO_2 adsorptions are analyzed by estimating their adsorption energies and charge transfers. The resulting values are compared with experimental desorption temperatures for NO and NO_2. The adsorption of the poisoning agent SO_2 is also analyzed. Optimum SnO_2 working temperatures for minimum SO_2 poisoning in NO_2 sensing applications are discussed from the perspective of adsorption. In all cases, we observe that the surface reduction state has noticeable consequences on adsorption strength. We also present an *ab initio* thermodynamics study to analyze the stability of several surface reduction configurations with respect to the ambient oxygen partial pressure and the temperature of the material. Finally, the interaction of NO_2 with spherical SnO_2 nanoparticles smaller than 2nm is considered.**

***Index Terms* — 1. Modeling and simulation of systems and properties of matter at the nanoscale: DFT, SnO_2, gas sensor, NO, NO_2, SO_2.**

I. Introduction

GAS sensor performance depends on the surface chemical activity of the active materials. The theoretical study of surface-adsorbate interactions provides a valuable tool for understanding the chemistry of gas sensors. Chemical transduction involves many stages, including the adsorption of the target species and charge transfer from the compound to the sensing material. These phenomena must be studied in order to understand the sensing process.

Tin dioxide (SnO_2) is one of the most common sensing materials in solid-state gas sensors [1]. It shows significant surface reactivity with reducing (CO, NO) and oxidizing gases (O_2, NO_2) [2,3]. The present work deals with adsorptions involved in the detection of NO_x using SnO_2. Detection of NO_x is important because it is a toxic environmental pollutant [4]. However, to explain the behavior of sensors, we need to keep in mind that certain processes may interfere with the sensor surfaces [5]. This interference can change the effective adsorptions of the target species and, therefore, their detection. In the case of the SnO_2 surface, SO_2 is one of the most important poisons [6]. The present analysis therefore considers the effects of SO_2 in order to point out the consequences of poisoning on sensing mechanisms.

Several papers have dealt with the energetics and the electron structure of stoichiometric and oxygen-defective SnO_2 surfaces [7-11]. The interaction of these surfaces with oxygen [12-14] and the presence of catalytic additives [15] have also been studied. To our knowledge, the interaction of NO_x with SnO_2 has only been analyzed in the case of the (101) and (100) surface orientations in a study on nanobelts [16].

We now present a theoretical study, partially reported in [17,18], of the interaction of NO_x with SnO_2-cassiterite in its most common surface orientation, which is shown to be the (110) [2] even in nanostructures [19]. Surface stability with respect to orientation and oxidized–reduced termination is discussed, the most significant adsorption sites of NO_x are identified and the energetics and charge transfers of the adsorption interaction are evaluated. We compare our results with data from desorption experiments where possible. The adsorption sites of SO_2 are also located and we discuss the effects of poisoning using technologically accessible parameters, such as the working temperature of a hypothetical SnO_2-based gas sensor. Finally, we present the first and promising results of an extension of this study, centered on ideal and infinite surfaces, to the case of SnO_2 nanoparticles.

II. Calculation Details

The first-principles methodology we used was based on density functional theory [20,21] (DFT) as implemented in the SIESTA code [22,23]. We used the generalized gradient approximation (GGA) for the exchange-correlation functional [24] and norm-conserving Troullier-Martins pseudopotentials [25] in Kleinman-Bylander factorization form [26]. Solutions of the Kohn-Sham's equations were expanded as linear combinations of atomic pseudo-wave-functions of finite range. For all atomic species double ζ plus polarization orbital basis-sets were used. Oxygen atoms were described by 6 valence electrons, nitrogen by 5, sulfur by 6 and tin atoms by 4 plus the corresponding pseudo-potential ion cores. We set a real space mesh cut-off [22,23] of 250Ry to obtain total energies converged within 5meV, which is more than sufficient for this kind of calculation [7]. In SIESTA, k-point sampling is controlled by the k-grid cut-off parameter defined as half the length of the smallest lattice vector of the supercell required to obtain the same sampling precision with a single k-point [27]. For bulk calculations, the total energy was converged to within 5meV per six-atom unit cell with a k-grid cut-off of 10 Å that generates a 5x5x7 Monkhorst-Pack set [28]. In slab calculations, k-point sampling in the direction normal to the surface is not needed, and all calculations were performed with a 5x5x1 Monkhorst–Pack set generated with a 15 Å k-grid cut-

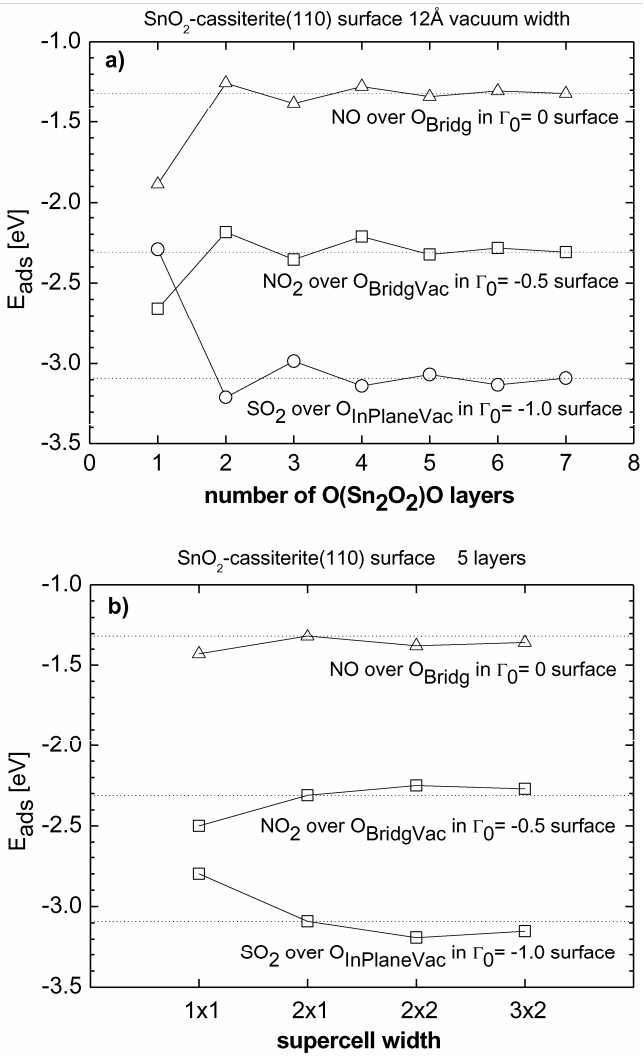

Fig. 1. *Adsorption energies (E_{ads}) of the three compounds studied (NO, NO_x and SO_2) onto an SnO_2-cassiterite (110) surface with different terminations, as function of: a) the number of O(Sn_2O_2)O layers and b) supercell width.*

off. Under these conditions, forces over atoms were converged to better than 0.004eV/Å^2. We also considered spin polarization in the total energy computations, and corrected the basis set superposition error [29] (BSSE) in the calculated adsorption energies.

To deal with surface stability, adsorption energy calculations and charge transfer estimations, we modeled all surface geometries as three dimensionally periodic slab systems, generated from the relaxed bulk unit cell, with a vacuum width of 12 Å between surfaces to avoid interaction between periodic images of the slabs [7-16].

Initially, to explore different possible adsorption sites, we performed calculations using slabs composed of two O(Sn_2O_2)O layers. For adsorption and structural calculations, we used slabs composed of five O(Sn_2O_2)O layers. Increasing the slab thickness to seven layers had a negligible effect on energetics and surface relaxations (see Figure 1.a). This procedure was successfully used in previous works [9,10,15]. Furthermore, we analyzed the influence of supercell width and showed that a 2x1 supercell provides converged adsorption energies (see Figure 1.b). Comparable supercell widths were previously employed in similar works [16].

We introduced structural relaxations by means of conjugate gradient minimization of the energy, until the forces on all the atoms (calculated as analytical derivatives of the total energy [30]) were smaller than 0.04eV/Å^2 (which is one order of magnitude greater than the estimated force convergence). In the relaxation of the slabs, supercell dimensions were kept constant and, as proposed by some authors [7], we choose to impose no constraints to the atomic positions within the supercell. In the slab composed of 5 layers, the maximum displacement of the atoms in the middle layer was as small as 0.05 Å.

To estimate charge transfers from/to admolecules, we computed partial charge on each atom using the Mulliken population analysis [31].

III. Results and Discussion

A. Surface orientation stability

It is commonly agreed that the facets of a crystal are those that minimize the total surface free energy (γ) of the system [32]. Consequently, for a given material, the most common (and relevant) facet orientation will have the lowest γ. Therefore, we calculated the surface free energies of several low index facets of SnO_2-cassiterite—also known as rutile, a tetragonal phase, space group $P4_2mnm$, lattice parameters a = b = 4.74Å c = 3.19Å and two non-symmetry-equivalent atoms at $(0.0,0.0,0.0)_{Sn}$ and $(0.305,0.305,0.0)_O$ [2]—in order to select the surface on which the adsorption processes would be analyzed. The low-index orientations we considered initially are (110), (100), (101) and (001), which are accepted as some of the most common SnO_2-cassiterite faceting surfaces [2,7].

Surface free energy values were calculated following the procedure and definitions described in [7,33], and we compare the results with values from the literature in Table I. Our calculated data are in acceptable agreement with the literature. We based our study on the (110) orientation since it has the lowest surface free energy. TiO_2 results are shown for comparison with another cassiterite system whose (110) orientation also has the lowest surface energy [34].

Figure 2 shows one of the slab models used for adsorption onto the SnO_2-cassiterite(110) surface. It clearly shows that it is possible to distinguish between bridging oxygen (O_{Bridg}) and in-plane oxygen ($O_{InPlane}$) [9]. When any one of these oxygen

TABLE I
CASSITERITE SURFACE FREE ENERGY RESULTS

Surface	γ [J/m^2] This work SnO_2 GGA <±0.20	SnO_2 GGA [7] <±0.20	TiO_2 LDA [34]
(110)	1.01	1.04	0.89
(100)	1.32	1.14	1.12
(101)	1.49	1.33	1.39
(001)	1.87	1.72	1.65

Surface free energy (γ) for the SnO_2-cassiterite facet orientations considered. Several references from the literature are given. Computational accuracy is also shown when possible.

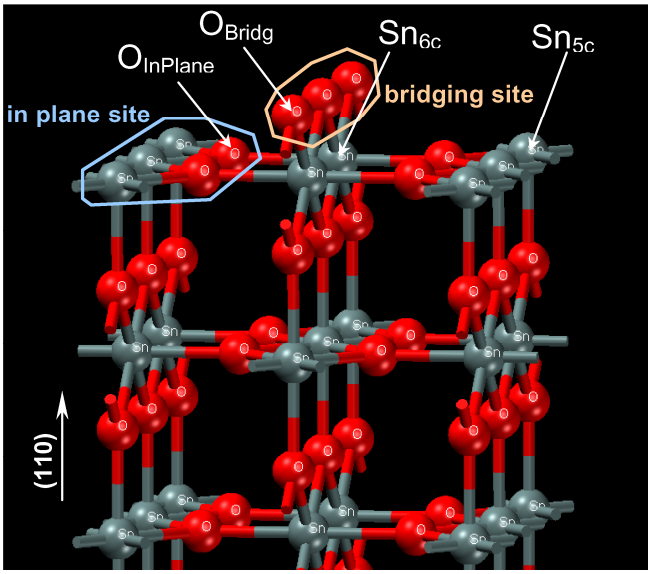

Fig. 2. *Slab model of the SnO_2-cassiterite (110) surface. Adsorption sites are highlighted and relevant surface atoms are identified.*

atoms is removed, a surface oxygen vacancy is generated. Henceforth, we will refer to these as $O_{BridgVac}$ and $O_{InPlaneVac}$, respectively.

B. Surface reduction/oxidation stability

We follow the methodology for the interpretation of *ab initio* calculations on surface models in terms of oxidation – reduction thermodynamics described by Reuter and Scheffler [35]. Briefly, the most stable surface composition and geometry at a given temperature T and pressure P is the one that minimizes the surface free energy σ(T,P) given by

$$\sigma(T,P) = \gamma - \Gamma_O \mu_O(T,P) /A \qquad (1)$$

where Γ_O = ½ (N_O – 2N_{Sn}) is the excess of oxygen in each surface (N_O and N_{Sn} are the number of oxygen and tin atoms in the outermost O(Sn_2O_2)O layer respectively), γ is the surface free energy at μ_O = 0 (i.e. under the ground conditions of 0K that are assumed in DFT), μ_O(T,P) is the oxygen chemical potential (that is given as a function of the temperature and the partial pressure of O_2 [36]) and A is the area of the slab model. In this procedure, *ab initio* calculations provide estimations of γ which can be used to evaluate the surface free energy, σ, of a particular surface termination (Γ_O) for a range of μ_O values that are functions of T and P. Two points must be considered to ensure that the μ_O values are physically meaningful: SnO_2 dissociates into SnO + O_2 at temperatures above 1500ºC [37] and, for gas sensing applications under ambient conditions, the oxygen partial pressure can be fixed at atmospheric conditions (i.e.: ~0.21bar). Therefore, μ_O to values must be restricted from –2.7eV (at 1500ºC and 0.21bar) to 0eV (at –273ºC).

Semancik and coworkers experimentally demonstrated that simple heating of a stoichiometric SnO_2-cassiterite(110) surface under UHV to temperatures above 225ºC leads to a loss of O_{Bridg} and the formation of bridging oxygen vacancies ($O_{BridgVac}$) [38,39]. However, if the temperature is raised above 525ºC, in-plane oxygen vacancies ($O_{InPlaneVac}$) can be produced, which usually form complex configurations with the presence of both $O_{BridgVac}$ and $O_{InPlaneVac}$. As stated in [38], it is worth noting that the given vacancy generation temperatures may depend on the particular samples used and the oxygen pressure. In any case, it is accepted that $O_{BridgVac}$ are generated at lower temperatures than $O_{InPlaneVac}$ and that the latter form more complex configurations [2].

Figure 3 shows straight line plots of σ(μ_O) for several surface terminations. It can be observed that for a single oxygen vacancy per slab unit (Γ_O = –0.5) $O_{BridgVac}$ becomes more stable than the stoichiometric configuration at 270ºC whereas $O_{InPlaneVac}$ does so at 480ºC (points α and β, respectively). Thus, the thermodynamics of the formation of a single $O_{BridgVac}$ is fairly well explained by *ab initio* calculations but (with the model used) it is not possible to determine the threshold temperature above which a single $O_{InPlaneVac}$ will be more stable than an $O_{BridgVac}$. In order to study this point, and bearing in mind the complex configurations suggested in [38], we considered double oxygen vacancies per slab termination (Γ_O = –1). All these complex configurations cross the single $O_{BridgVac}$ line at temperatures between 640 and 780ºC (point δ).

In short, under ambient conditions, the stoichiometric surface configuration is the most stable, as we expected. When the temperature is raised above 270ºC a single $O_{BridgVac}$ may form and even at higher temperatures (above 480ºC) the formation of a single isolated $O_{InPlaneVac}$ is plausible. At temperatures above 640ºC multi-vacant configurations are the most probable. This predicted evolution is compatible with the known behavior with slightly higher temperatures than under UHV conditions as expected due to the presence of ambient oxygen that may make vacancy generation more difficult. All this suggests that temperature can be used to technologically adjust the surface oxygen vacancy type and concentration.

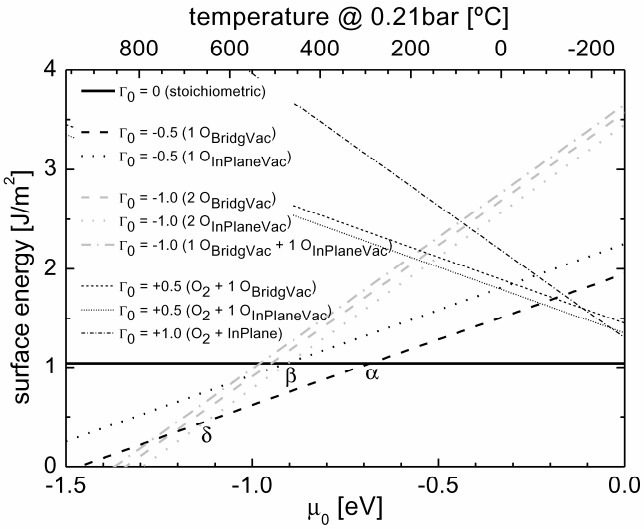

Fig. 3. *Surface free energies for different terminations of the SnO_2(110) surface as a function of the oxygen chemical potential. The top axis shows the corresponding O_2 gas temperature for atmospheric air equivalent conditions (i.e.: oxygen partial pressure of ~0.21bar) [35].*

TABLE II
ADMOLECULES' MODELING VERIFICATION

Compound	Bond energy [eV]		Bond length [Å]		Angle [º]	
	This work	Ref.[40]	This work	Ref.	This work	Ref.
O_2	5.90	6.23 (calc.) 5.23 (exp.)	1.24	1.18 – 1.21 [41]	–	–
N_2	9.47	10.55 (calc.) 9.47 (exp.)	1.12	1.09 – 1.11 [42]	–	–
NO	7.03	7.45 (calc.) 6.63 (exp.)	1.17	1.12 – 1.17 [43]	–	–
NO_2	5.54	–	1.23	1.20 [44]	132	133-134 [44]
SO_2	5.91	–	1.49	1.48 [45]	112	109 [45]

Energetic and geometric first-principles modeled parameters of several molecules involved in the adsorptions considered in this work. Reference values are from the literature.

To give a more complete view of the surface stability, we considered several oxidized configurations and, remarkably, these are metastables in the complete range of temperatures under atmospheric oxygen partial pressure. The difficulty in oxidizing the surface may rise from the fact that the cations in SnO_2 are already in their maximum oxidation states, which prevents the further addition of monatomic O^{2-} species to the surface.

We should stress that, because of the size of the slab used in our calculations (2x1 supercell), here we have compared only certain discrete degrees of oxidation – reduction of the surface. For example, in the case of $O_{BridgVac}$, $\Gamma_O = -0.5$ and $\Gamma_O = -1$ correspond to 50% and 100% reduction of the surfaces, but, in the real system, intermediate compositions may be stable under different pressure and temperature conditions. Slightly reduced surfaces could then be stable at temperatures lower than those estimated above.

C. Adsorption onto SnO_2(110)

To estimate the energy change and the charge transfer involved in the process of adsorption of a molecule onto a clean surface, we built models of 1) the clean surface slab, 2) the molecule, and 3) the surface plus the molecule system. For all three of these models, total energy calculations were performed, allowing us to evaluate the total energy balance of the adsorption process (the so-called adsorption energy, E_{ads}):

$$E_{Tinitial} = E_{T(clean\ surface)} + E_{T(molecule)}$$
$$E_{Tfinal} = E_{T(clean\ surface+molecule)}$$
$$E_{ads} = \Delta E_T = E_{Tfinal} - E_{Tinitial} \qquad (2)$$

A negative E_{ads} means that the adsorption is energetically favorable, and may occur spontaneously without entropic considerations (DFT deals with the ground state at 0K).

The charge transfer between the surface and the adsorbed molecule (Δq) was evaluated comparing the valence charge associated to the molecule in the isolated case with the adsorbed configuration.

The adsorption analysis requires several complementary steps: identification of possible surface adsorption sites (considering vacant sites), molecular modeling and finally, adsorption modeling of NO_x and SO_2.

Two relevant adsorption sites appear to be a natural choice for the stoichiometric surface: a bridging site and an in-plane site [9]. It seems clear that the latter involves not only oxygen atoms but also the corresponding Sn_{5c} atom. In addition, the adsorption to oxygen-removed sites (vacant sites) seems relevant, so $O_{BridgVac}$ and $O_{InPlaneVac}$ sites are considered.

A good description of the adsorbed molecules is necessary to obtain credible theoretical predictions, Table II gives the molecular models used and the energetic and geometric parameters obtained compared with those in the literature. The agreement achieved is comparable with the commonly accepted discrepancy described in the literature [40].

Table III summarizes calculated E_{ads} and Δq for NO and NO_2 and the adsorption sites considered. Adsorption temperatures are obtained by means of the well-known Redhead equation, which links the $|E_{ads}|$ of a process with its maximum desorption rate temperature (T_{MDR}) in a temperature-programmed desorption (TPD) experiment [46]. The adjusting parameters were set according to the experimental conditions of [47] where an experimental TPD spectrum can be found for NO and NO_2 desorption from an SnO_2(110) surface (Figure 4).

We recall that our model only provides energies (and their corresponding desorption temperatures) for the specific adsorption configurations analyzed. In contrast, an experimental TPD spectrum provides the temperature range over which species are desorbed by considering a plethora of adsorption configurations present in a real sample. Consequently, we would expect the calculated temperatures to belong to the corresponding experimental TPD signal range. Our theoretical predictions of T_{MDR} for the few adsorption cases considered fall within the wide experimental desorption peaks from [47].

Our results suggest that O_{Bridg} sites are the most energetically favorable for NO. This behavior is comparable with the observation that NO reduces SnO_2, given that NO is expected to bond with a surface oxygen and eventually to remove it, thus reducing the surface [1]. In contrast, energetically preferred adsorption sites for NO_2 are related to oxygen vacancies. Moreover, the TPD spectrum simulated for NO_2 suggests that the lower temperature peak could be associated with $O_{InPlaneVac}$ sites while the one at a higher temperature seems to be due to $O_{BridgVac}$.

It is important to notice that the difference between the preferred adsorption sites of NO and NO_2 indicates that by generating vacant sites and adjusting their density, the feasibility of adsorption onto SnO_2 of NO versus NO_2 may be changed.

TABLE III
NO AND NO_2 ADSORPTION ONTO SnO_2(110)

Adsorbate	Surface termination (Γ_O)	Adsorption site	E_{ads} [eV]		T_{MDR} [ºC]		Δq [e^-]
NO	0.0	O_{Bridg}		–1.32	198	(a)	–0.21
	0.0	$Sn_{InPlane}$		–0.24	52	(b)	–0.02
	–0.5	O_{Bridg}		–1.18	167	(c)	–0.24
	–0.5	O_{Bridg} + (SO_2 in $O_{BridgVac}$)		–1.28	–	(ϒ)	
	–0.5	$O_{BridgVac}$		–0.42	89	(d)	–0.05
	–1.0	$O_{BridgVac}$		–0.98	153	(e)	–0.10
NO_2	0.0	O_{Bridg}		+1.51	–		–
	0.0	$Sn_{InPlane}$		–0.52	94	(t)	+0.42
	–0.5	$O_{BridgVac}$	(single bonded)	–2.31	502	(u)	+0.31
	–0.5	$O_{BridgVac}$-$Sn_{InPlane}$		+0.34	–		–
	–1.0	$O_{BridgVac}$	(single bonded)	–2.02	424	(v)	+0.65
			(double bonded)	–1.95	400	(w)	+0.57
	–1.0	$O_{BridgVac}$-$Sn_{InPlane}$		–2.11	454	(x)	+0.68
	–0.5	$O_{InPlaneVac}$	(single bonded)	–1.26	178	(y)	+0.61
	–1.0	$O_{InPlaneVac}$	(double bonded)	–0.74	120	(z)	+0.92

Calculated adsorption energies (E_{ads}) and charge transfers (Δq) for NO_x onto several adsorption sites of the SnO_2(110) surface and maximum desorption rate temperature (T_{MDR}) estimated for the experimental conditions of [47]. Some configurations are not energetically favorable (E_{ads} > 0). Energetically favorable processes are labeled with letters in parenthesis in order to identify them in Fig. 4. For NO, a configuration in the presence of SO_2 (ϒ) is considered for later discussion on poisoning.

As far as the charge transfer Δq is concerned, the calculations predict that while NO releases charge to the underlying material, NO_2 captures it: this is compatible with the usual interpretation of the electrical response of gas sensors based on metal oxides. According to it, a reducing gas (such as NO) is expected to reduce the resistance of the sensing metal oxide due to a donation of e^- to the conduction states of the metal oxide; the opposite is expected for an oxidizing gas (such as NO_2).

In the case of NO_2, it is also remarkable that the adsorptions onto $O_{BridgVac}$ arise Δq values smaller than those where an in-plane site is involved. This is compatible with the fact that the maximum response of SnO_2 sensors to NO_2 is found at working temperatures from 100 to 250 ºC [1] (approximately the range of the lower temperature peak of the TPD spectrum).

Table IV summarizes the calculated E_{ads} for SO_2 at several sites. As for NO_2, the preferred adsorption sites involve oxygen vacancies but in this case it seems that the adsorption has a similar strength for both $O_{InPlaneVac}$ and $O_{BridgVac}$. This difference in behavior with regard to the oxygen vacancy type has dramatic consequences on the interference of SO_2 when trying to detect NO_2.

It is known that SO_2 avidly saturates NO_2 adsorption sites, reducing the sensing capability of SnO_2 [6]. In the present calculations, the strongest adsorption within the cases studied corresponds to SO_2. This theoretical behavior is compatible with the experimental evidence of poisoning.

In particular, SO_2 adsorbs more strongly than NO_2 to vacant oxygen sites but the difference in the calculated E_{ads} values is smaller for $O_{BridgVac}$ related adsorptions (the higher temperature peak in the NO_2 TPD spectrum). This suggests that the poisoning strength depends on the adsorption site involved in the process. So SnO_2(110) surfaces, in which the presence of $O_{BridgVac}$ dominates and there are few $O_{InPlaneVac}$, would appear to be a better sensor candidate as it should experience less poisoning. Linking this with the surface reduction stability described above, it is clear that in order to avoid the massive apparition of $O_{InPlaneVac}$ the temperature of the sensing material should not exceed 480ºC. If an occasional single $O_{InPlaneVac}$ is present below this temperature, adsorption onto such a site should be avoided to diminish the effect of the poisoning, and so the sensing material should work at temperatures higher than 200ºC which favors the desorption of NO_2 from and $O_{InPlaneVac}$. Finally, to obtain good sensing behavior over a large range of the target gas concentration,

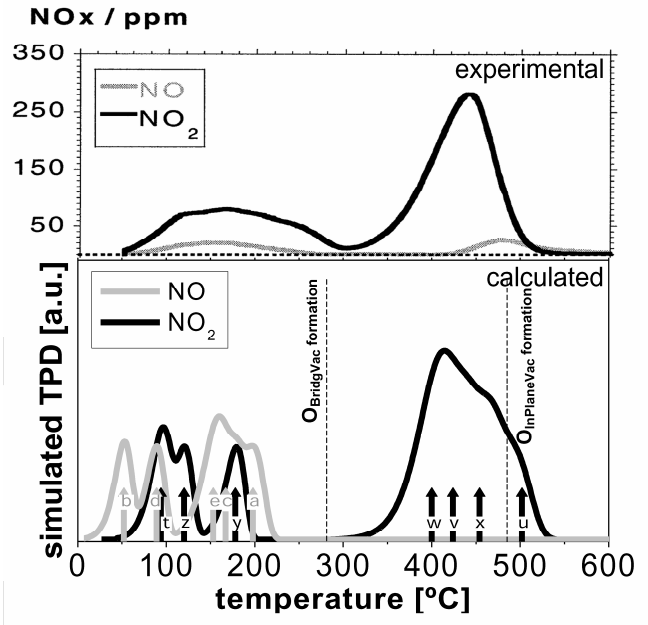

Fig. 4. *Top: Experimental TPD spectra for NO and NO_2 desorbing from a dehydroxylated SnO_2(110) surface (Reprinted from [47]). Bottom: Calculated TPD spectra for NO and NO_2 considering all the configurations detailed in Table III. One TPD spectrum was simulated (by means of solving the rate expression for desorption kinetics [46,48]) for each adsorption configuration with the experimental parameters given in [47]. For every configuration, the temperature corresponding to the maximum desorption rate is indicated with a labeled arrow (see labels and T_{MDR} values in Table III). Total spectra are sums of the normalized single configuration spectra. Total intensities only serve as a visual guide as they are obtained from summing normalized intensities.*

TABLE IV
SO_2 ADSORPTION ONTO SnO_2(110)

Adsorbate	Surface termination (Γ_O)	Adsorption site	E_{ads} [eV]		T_{MDR} [ºC]	Δq [e$^-$]
SO_2	0.0	O_{Bridg}		+1.72	–	–
	0.0	$Sn_{InPlane}$		–0.86	128	+0.50
	–0.5	$O_{BridgVac}$	(single bonded)	–2.05	435	+0.43
	–0.5	$O_{BridgVac}$-$Sn_{InPlane}$		+1.12	–	–
	–1.0	$O_{BridgVac}$	(single bonded)	+0.26	–	–
			(doble bonded)	–2.56	606	+0.72
	–1.0	$O_{BridgVac}$-$Sn_{InPlane}$		–2.97	741	+0.95
	–0.5	$O_{InPlaneVac}$	(single bonded)	–2.98	748	+0.53
	–1.0	$O_{InPlaneVac}$	(doble bonded)	–3.09	770	+0.69

Calculated adsorption energies (E_{ads}) and charge transfers (Δq) for SO_2 onto several adsorption sites of the SnO_2(110) surface and maximum desorption rate temperature T_{MDR} estimated for the experimental conditions of [47]. Notice that, in contrast to the case of NO_2, our calculations show that SO_2 adsorption onto a 100% reduced slab may only be spontaneous ($E_{ads} < 0$) in one single O bonding configuration. Some configurations are not energetically favorable ($E_{ads} > 0$).

adsorption sites must be kept unsaturated. In other words, the sensing material should work at a high desorption rate temperature to achieve a steady state where the adsorption/desorption ratio is a function of concentration. Consequently, according to the NO_2 TPD spectrum, temperatures between 200 and 300ºC do not appear very promising.

All these considerations suggest that to achieve the best adsorption conditions and diminish poisoning by SO_2, the optimum working temperatures are between 300ºC to 450ºC (left side of the high temperature desorption peak of NO_2).

The preferred adsorption sites for NO are O_{Bridg}. Therefore, it may seem that there is no competitive behavior with SO_2. However, Table III shows that, for intermediate reductions, the adsorption of NO onto O_{Bridg} in the presence of an SO_2 occupying an $O_{BridgVac}$ site (Table III case ϒ) is slightly stronger than in the non-interacting case (case c). These results suggest that in spite of the predilection for different adsorption sites shown by NO and SO_2, a cross-influence may occur between the two compounds, and this would merit further analysis.

It is important to bear in mind that the previous discussion is centered on good behavior in the adsorption and charge transfer stages. These are only two stages in the chemical transduction and therefore they are necessary but not sufficient to guarantee a good sensing response.

As a final remark, the previous discussion makes evident the key role of surface oxygen vacancies in the surface interactions behind gas sensing with SnO_2. Recently, we have proposed that the luminescence signal of SnO_2 [49] (and, possibly, other metal oxides such as ZnO [50]) can be used to monitor its surface reduction/oxidation state.

D. Adsorption onto SnO_2 nanoparticles

In the last years, the use of nanostructured materials, with increased surface/volume ratio, has been one of the most fruitful strategies to improve the performance of gas sensors based on metal oxides [51]. Outstanding performances have been obtained in commercial sensors with nanoparticles smaller than 3nm [51]. Consequently, the validity of the approximation of perfect and infinite surfaces of SnO_2 (which is appropriate for polycrystalline gas sensors with gain sizes above of hundreds of nanometers) should be revised for the smaller nanoparticles. Hereunder, we present our first results on the interaction of NO_2 with SnO_x spherical nanoparticles of 1.0, 1.1, 1.8 and 1.9 nm in diameter. These sizes produce SnO_2 nanoparticles terminated with SnO_2(110)-like facets that ease the comparison with the previous calculations.

Table V summarizes the calculated gap energies (E_{gap}), the enthalpies of formation (ΔH) of bulk (fully coordinated) and surface (in a bridging coordination) oxygen atoms, and E_{ads} and Δq for NO_2 adsorptions onto $O_{BridgVac}$ sites (the strongest adsorption configuration detected previously).

Results predict a widening of the E_{gap} when reducing the nanoparticle down to the nanometer range. This is the expected behavior due to the quantum confinement of the electrons inside a nanoparticle surrounded by vacuum.

Besides, the enthalpy of formation of both bulk and surface O vacancies diminishes with the nanoparticle dimensions. Similar trends have been observed experimentally in other metal oxides, such as CeO_2 [52].

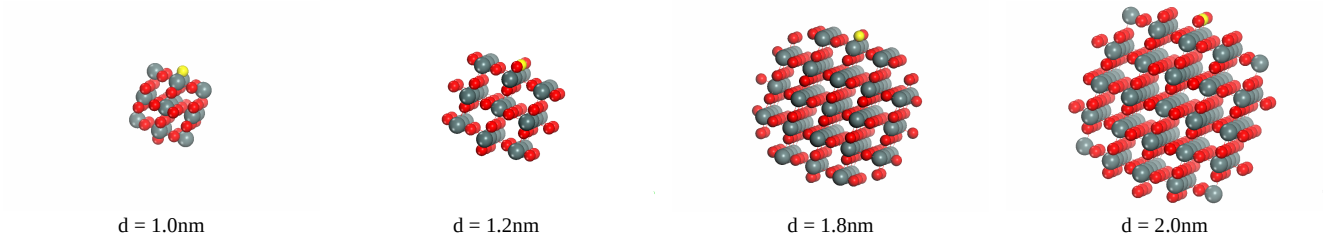

Fig. 5. *Atomistic model of the four spherical SnO_x nanoparticles we studied. Calculation results are presented in Table V. Gray and red balls correspond to tin and oxygen atoms, respectively. Atoms in green highlight the bridging site where an $O_{BridgVac}$ was generated and NO_2 was adsorbed.*

TABLE V
SnO_X NANOPARTICLES RESULTS

diameter [nm]	n_{atoms}	x	E_{gap} [eV]	$\Delta H\ O_{BulkVac}$ [eV]	$\Delta H\ O_{BridgVac}$ [eV]	NO_2 over $O_{BridgVac}$	
						E_{ads} [eV]	Δ_q [e–]
1.0	51	2.4	1.72	3.78	2.39	-4.22	+0.92
1.2	83	1.8	1.70	3.85	2.46	-4.01	+0.91
1.8	271	1.9	1.65	4.12	3.54	-3.53	+0.89
2.0	351	2.0	1.64	4.15	3.62	-3.51	+0.89
crystal	∞	2.0	1.60	4.40	3.85	-2.02	+0.85

Calculated gap energies (E_{gap}) enthalpies of formation of oxygen vacancies in bulk-like coordination ($\Delta H\ O_{BulkVac}$), and surface bridging coordination ($\Delta H\ O_{BulkVac}$) for 4 spherical nanoparticles of SnO_x. Adsorption energies (E_{ads}) and charge transfers (Δq) for NO_2 onto $O_{BridgVac}$ sites of the nanoparticles are also presented. Besides the diameters, an the number of atoms contained in the atomistic models (n_{atoms}), the exact composition (x) of each nanoparticle is shown. Results corresponding to the (semi-)infinite crystal (either the surface, or the bulk) are given as reference.

As regards the interaction with NO_2, an increase of both the strength and the charge transfer of the adsorption is predicted when reducing the nanoparticles' diameter.

All these results suggest a strong influence of the nanoparticle size, not only on the intrinsic properties of SnO_2 but also on its interaction with gases. In any case, further work is needed to verify the influence of the shape of the nanoparticle (cleavages based on the Wulff's construction of SnO_2 could be a good option) or its stoichiometry and to consider other adsorption configurations. In the near future, the possibility of exploring the few-nanometer range thanks to new computational facilities and codes could also be enlightening.

The interaction of NO_2 with SnO_2 nanoparticles between 1 and 2 nm in diameter has been explored in order to check the validity of the approximation of infinite surface when modeling extremely small nanoparticles. The results suggest a strong influence on the interaction between NO_2/SnO_2 but further work is needed for a complete comprehension of its effects.

We have shown how *ab initio* modeling of surfaces and adsorptions can provide ideas to improve the performance of solid-state chemical sensors. Theoretical predictions regarding optimum working conditions for real sensors would require a more complex model including, for example, the cross-influence of OH groups due to humidity.

IV. CONCLUSION

We adopt a theoretical approach to study the NO and NO_2 adsorption onto SnO_2(110) based on *ab initio* calculations. Bridging oxygen sites and oxygen vacancy sites were identified as the most relevant adsorption sites for NO and NO_2 respectively. This difference suggests that by adjusting the oxygen vacancy site density the feasibility of NO versus NO_2 adsorption onto SnO_2 may be changed.

Oxygen vacancies seem to be the most favorable adsorption sites for poisoning by SO_2, suggesting competitive behavior with NO_2. Theoretical trends indicate that while SO_2 adsorption strength is almost independent of the oxygen vacancy type (bridging or in-plane), NO_2 adsorbs more strongly onto bringing than in-plane vacancies. Such a difference suggests that poisoning may be reduced if the working conditions make bridging oxygen vacancies the dominant adsorption site. Considering the surface reduction stability with respect to temperature under atmospheric oxygen partial pressure, and the experimental and *ab initio* modeled TPD spectra of NO_2, ideal SnO_2(110) surfaces present optimum adsorption activity for gas sensing applications at temperatures between 300 and 450ºC. In the case of NO, no competitive behavior with SO_2 is expected due to their predilection for different adsorption sites, but further study may be necessary to analyze cross-influences.

Maximum charge transfers from SnO_2(110) to the adsorbed NO_2 are predicted for interactions involving in-plane sites, in good agreement with the maximum responses of the sensors which are obtained at working temperatures corresponding also to interactions with in-plane sites.

ACKNOWLEDGMENT

The author is grateful to Prof. F. Illas and Prof. K.M. Neyman (Universitat de Barcelona, Spain) for enlightening discussions and Dr. J.M. Pruneda and Prof. P. Ordejón (ICMAB-CSIC, Spain) for their help in the first steps of the *ab initio* calculations. The computer resources, technical expertise and assistance provided by the Barcelona Supercomputing Center - Centro Nacional de Supercomputación and the Supercomputation Center of Catalonia are thakfully acknowledged. This work was partially funded by the European Integrated Project NANOS4 (MMP4-CT-2003-001528) of the 6th EU Framework Program and the CICyT National Project MAGASENS. Finally, J.D.P. acknowledges the support of the FPU program of the Spanish Ministry of Education and Science.

REFERENCES

[1] W. Göpel and K.D. Schierbaum, "SnO_2 sensors: Current status and future prospects", *Sens. Actuators, B*, vol. 26, pp. 1-12, May 1995.

[2] M. Batzill and U. Diebold, "The surface and materials science of tin oxide", *Prog. Surf. Sci.*, vol. 79, pp. 47-154, Nov. 2005.

[3] G. Sverveglieri, "Recent developments in semiconducting thin-film gas sensors", *Sens. Actuators, B*, vol. 23, pp. 103-109, Feb. 1995.

[4] A. Fritz and V. Pitchon, "The current state of research on automotive lean NO_x catalysis", *Appl. Catal., B*, vol. 13, pp. 1-25, Sep. 1997.

[5] D.E. Williams , G.S. Henshaw and K.F.E. Pratt, "Detection of sensor poisoning using self-diagnostic gas sensors", *J. Chem. Soc. - Faraday Transactions*, vol. 91, pp. 3307-3308, May. 1995.

[6] B. Ruhland, T. Becker, G. Muller, "Gas-kinetic interactions of nitrous oxides with SnO_2 surfaces", *Sens. Actuators, B*, vol. 50, pp. 85-94, Jul. 1998.

[7] J. Oviedo and M.J. Gillan, "Energetics and structure of stoichiometric SnO_2 surfaces studied by first-principles calculations", *Surf. Sci.*, vol. 463, pp. 93-101, Sep. 2000.

[8] J. Oviedo and M.J. Gillan, "The energetics and structure of oxygen vacancies on the $SnO_2(110)$ surface", *Surf. Sci.*, vol. 467, pp. 35-48, Nov. 2000.

[9] M.A. Mäki-Jaskari and T.T. Rantala, "Band structure and optical parameters of the $SnO_2(110)$ surface", *Phys. Rev. B*, vol. 64, p. 075407, Jul. 2001.

[10] M.A. Mäki-Jaskari and T.T. Rantala, "Theoretical study of oxygen-deficient $SnO_2(110)$ surfaces", *Phys. Rev. B*, vol. 65, p. 245428, Jun. 2002.

[11] M. Batzill, K. Katsiev, J.M. Burst, U. Diebold, A.M. Chaka and B. Delley, "Gas-phase-dependent properties of $SnO_2(110)$, (100), and (101) single-crystal surfaces: Structure, composition, and electronic properties", *Phys. Rev. B*, vol. 72, p. 165414, Oct. 2005.

[12] J. Oviedo and M.J. Gillan, "First-principles study of the interaction of oxygen with the $SnO_2(110)$ surface", *Surf. Sci.*, vol. 490, pp. 221-236, Sep. 2001.

[13] J. Oviedo and M.J. Gillan, "Reconstructions of strongly reduced $SnO_2(110)$ studied by first-principles methods", *Surf. Sci.*, vol. 513, pp. 26-36, Jul. 2002.

[14] F.R. Sensato, R. Custódio, M. Calatayud, A. Beltrán, J. Andrés, J.R. Sambrano and E. Longo, "Periodic study on the structural and electronic properties of bulk, oxidized and reduced $SnO_2(110)$ surfaces and the interaction with O_2", *Surf. Sci.*, vol. 511, pp. 408-420, Jun. 2002.

[15] M.A. Mäki-Jaskari and T.T. Rantala, "Density functional study of Pd adsorbates at $SnO_2(110)$ surfaces", *Surf. Sci.*, vol. 537, pp. 168-178, Jul. 2003.

[16] A. Maiti, J.A. Rodriguez, M. Law, P. Kung, J.R. McKinney and P. Yang, "SnO_2 Nanoribbons as NO_2 Sensors: Insights from First Principles Calculations", Nano Lett., vol. 3, pp. 1025-1028, Jun. 2003.

[17] J.D. Prades, A. Cirera, J.R. Morante, J.M. Pruneda and P. Ordejón, "Ab initio study of NO_x compounds adsorption on SnO_2 surface", presented at the European Materials Research Society Spring Meeting, Nice, France, May 27- June 2, 2006. In press in *Sens. Actuators, B.*

[18] J.D. Prades, A. Cirera and J.R. Morante, "First-Principles Study of NO_x and SO_2 Adsorption onto $SnO_2(110)$", *J. Electrochem. Soc.*, vol. 154, pp. H657-H680, May 2007.

[19] J. Arbiol, A. Cirera, F. Peiró , A. Cornet, J.R. Morante, J.J. Delgado and J.J. Calvino, "Optimization of tin dioxide nanosticks faceting for the improvement of palladium nanocluster epitaxy", *Appl. Phys. Lett.*, vol. 80, pp. 329-331, Jan. 2002.

[20] P. Hohenberg and W. Kohn, "Inhomogeneous Electron Gas", *Phys. Rev.*, vol. 136, pp. B864-B871, Nov. 1964.

[21] W. Kohn and L.J. Sham, "Self-Consistent Equations Including Exchange and Correlation Effects", *Phys. Rev.*, vol. 140, pp. A1133-A1138, Nov. 1965.

[22] P. Ordejón, E. Artacho, and J.M. Soler, "Self-consistent order-N density-functional calculations for very large systems", *Phys. Rev. B*, vol. 53, pp. R10441-R10444, Apr. 1996.

[23] J.M. Soler, E. Artacho, J.D. Gale, A. García, J. Junquera, P. Ordejón and D. Sánchez-Portal, "The SIESTA method for ab initio order-N materials simulation", *J. Phys.: Condens. Matter*, vol. 14, pp. 2745-2779, Mar. 2002.

[24] J.P. Perdew, K. Burke and M. Ernzerhof, "Generalized Gradient Approximation Made Simple", *Phys. Rev. Lett.*, vol. 77, pp. 3865-3868, Oct. 1996.

[25] N. Troullier and J. L. Martins, "Efficient pseudopotentials for plane-wave calculations", *Phys. Rev. B*, vol. 43, pp. 1993-2006, Jan. 1991.

[26] L. Kleinman and D.M. Bylander, "Efficacious Form for Model Pseudopotentials", *Phys. Rev. Lett.*, vol. 48, pp. 1425-1428, May. 1982.

[27] J. Moreno and J.M. Soler, "Optimal meshes for integrals in real- and reciprocal-space unit cells", *Phys. Rev. B*, vol. 45, pp. 13891-13898, Jun. 1992.

[28] H. Monkhorst and J. Pack, "Special points for Brillouin-zone integrations", *Phys. Rev. B*, vol. 13, pp. 5188-5192, Jun. 1976.

[29] S.F. Boys and F.F. Bernardi, "The calculation of small molecular interactions by the differences of separate total energies. Some procedures with reduced errors", *Mol. Phys.*, vol. 19, pp. 553-566, Oct. 1970.

[30] D. Sánchez-Portal, P. Ordejón, E. Artacho, J. M. Soler, "Density-functional method for very large systems with LCAO basis sets", *Int. J. Quantum Chem.*, vol. 65, pp. 453-461, Dec. 1997.

[31] A. Szabo, N. S. Ostlund, *Modern Quantum Chemistry*, New York: Dover, 1996, p. 151.

[32] A.S. Barnard and P. Zapol., "Effects of particle morphology and surface hydrogenation on the phase stability of TiO_2", *Phys. Rev. B*, vol. 70, p. 235403, Dec. 2004.

[33] W. Zhu and P.Wu, "Surface energetics of hydroxyapatite: a DFT study", *Chem. Phys. Lett.*, vol. 396, pp. 38-42, Aug. 2004.

[34] M. Ramamoorthy, D. Vanderbilt and R..D. King-Smith, "First-principles calculations of the energetics of stoichiometric TiO_2 surfaces", *Phys. Rev. B*, vol. 49, pp. 16721-16727, Jun. 1994.

[35] K. Reuter and M. Scheffler, "Composition, structure, and stability of $RuO_2(110)$ as a function of oxygen pressure", *Phys. Rev. B*, vol. 65, p. 035406, Dec. 2002.

[36] M.W. Chase, *NIST-JANAF Thermochemical Tables*, Woodbury: American Chemical Society, 1998.

[37] K. Ellmer, "Resistivity of polycrystalline zinc oxide films: current status and physical limit", *J. Phys. D: Appl. Phys.*, vol. 34, pp. 3097-3108, Oct. 2001.

[38] D.F. Cox, T.B. Fryberger and S. Semancik, "Oxygen vacancies and defect electronic states on the $SnO_2(110)$-1×1 surface", *Phys. Rev. B*, vol. 38, pp. 2072-2083, Jul. 1988.

[39] D.F. Cox, T.B. Fryberger and S. Semancik, "Preferential isotopic labeling of lattice oxygen positions on the $SnO_2(110)$ surface", *Surf. Sci.*, vol. 227, pp. L105-L108, Mar. 1990.

[40] S. Kurth, J.P. Perdew and P. Blaha, "Molecular and solid-state tests of density functional approximations: LSD, GGAs, and meta-GGAs", *Int. J. Quantum Chem.*, vol. 75, pp. 889-909, Oct. 1999.

[41] H. Dong, Y.-H. Ding and C.-C. Sun, "Mechanism of HCS + O_2 reaction: Hydrogen- or oxygen-transfer?", *Phys. Chem. Chem. Phys.*, vol. 7, pp. 3711-3715, Sep. 2005.

[42] H. Orita and N. Itoh, "Adsorption of N_2 and N_2O on Ni(755) surface: ab initio periodic density functional study", *Surf. Sci.*, vol. 550, pp. 166-176, Feb. 2004.

[43] Z.-G.Wei, X.-R. Huang, S.-W. Zhang, Y.-B. Sun, H.-J. Qian and C.-C. Sun, "A Theoretical Study on the Potential Energy Surface of the $^3C_2$ + NO Reaction", *J. Phys. Chem. A*, vol. 108, pp. 6771-6777, Jul. 2004.

[44] J.-X. Zhang, J.-Y. Liu, Z.-S. Li and C.-C. Sun, "Theoretical study on reaction mechanism of the fluoromethylene radical with nitrogen dioxide", *J. Comp. Chem.*, vol. 25, pp. 1888-1894, Nov. 2004.

[45] K. Sendt and B.S. Haynes, "Role of the Direct Reaction H_2S + SO_2 in the Homogeneous Claus Reaction", J. Phys. Chem. A, vol .109, pp. 8180-8186, Aug. 2005.

[46] M.C. Desjonquères and D. Spanjard, *Concepts in Surface Physics* (2nd ed.) Berlin: Springer, 1996.

[47] E. Leblanc, L. Perier-Camby, G. Thomas, R. Gibert, M. Primet and P. Gelin., "NO_x adsorption onto dehydroxylated or hydroxylated tin dioxide surface. Application to SnO_2-based sensors", *Sens. Actuators, B*, vol. 62, pp. 67-72, Jan. 2000.

[48] V.P. Zhdanov and B. Kasemo, "Simulation of oxygen desorption from Pt(111)", *Surf. Sci.*, vol. 415, pp. 403-410, Oct. 1998.

[49] J.D. Prades, J. Arbiol, A. Cirera, J.R. Morante, M. Avella, L. Zanotti, E. Comini, G. Faglia and G. Sberveglieri, "Defect study of SnO_2 nanostructures by cathodoluminescence analysis", *Sens. Actuators, B*, article in press, Oct. 2006.

[50] J.D. Prades, A. Cirera, J.R. Morante, A. Cornet, "Ab initio insights into the visible luminescent properties of ZnO", *Thin Sol. Films*, article in press, May 2007.

[51] E. Comini, "Metal oxide nano-crystals for gas sensing", *Anal. Chim. Acta*, vol. 568, pp. 28-40, May. 2006

[52] T. Suzuki, I. Kosacki, H.U. Anderson and P. Colomban, "Electrical Conductivity and Lattice Defects in Nanocrystalline Cerium Oxide Thin Films", *J. Am. Ceram. Soc.*, vol. 84, pp. 2007-2014, Jun. (2001)